PROCEEDINGS OF SPIE

Bistable silicon photonic MEMS switches

Sattari, Hamed, Toros, Adrien, Graziosi, Teodoro , Quack, Niels

SPIE.

Bistable silicon photonic MEMS switches

Hamed Sattari*[a], Adrien Toros[a], Teodoro Graziosi[a], Niels Quack[a]

[a]EPFL STI IMT GR-QUACK, Station 17, CH-1015 Lausanne, Switzerland

ABSTRACT

We present the design of a non-volatile, bistable silicon photonic MEMS switch. The switch architecture builds on our previously demonstrated silicon photonic MEMS switch unit cell, using vertically movable adiabatic couplers. We here propose to exploit compressive stress in the movable polysilicon waveguides in a controlled manner, to intentionally displace the movable waveguides out of plane upon release. We design the waveguide suspensions to achieve close alignment with the fixed bus waveguide in the ON state, and positioning of the movable waveguide far from the fixed waveguide in the OFF state. Both ON and OFF positions are stable mechanically, without the need for maintaining an actuation voltage. In order to actuate the movable waveguide, we design vertical comb drive actuators that allow to commutate between both stable ON and OFF positions. Finite Element simulations predict electrostatic switch actuation with less than 30 V for compressive stress typically accessible in deposited polysilicon thin films. We validate the bistability mechanism by comparison with a representative experimental demonstrator. The demonstrator consists of a structured 100 nm poly-Si layer, deposited by chemical vapor deposition onto a thermally oxidized (1 µm) silicon wafer, exhibiting a compressive intrinsic stress of 275 MPa. Upon direct writing laser based photolithography, etching and final HF vapor release, the suspended structures bend into either stable position, and we measure a total buckling amplitude of 800 nm, sufficient to entirely de-couple the waveguides optically in the OFF state.

Keywords: Silicon photonic, MEMS, bistable, switching, compressive stress, buckling

1. INTRODUCTION

Mechanical bistability has been recognized as a useful mechanism to engineer low-power consumption Micro-Electro-Mechanical Systems (MEMS) and has been widely implemented previously in applications such as mechanical memories [1], DC switches [2], and fiber-optical switches [3]. Mechanical bistability is particularly attractive for the design of low-power consumption systems, as it offers the possibility to address non-volatile states by means of mechanical latching into stable positions, providing access to a mechanical 'memory'. In microsystems technology, intrinsic stresses are typically encountered in deposited thin films. While it is usually desirable to minimize intrinsic stress in typical MEMS devices to prevent undesired deformations and related device failure, compressive stress can be exploited to deliberately design buckling beams, to implement bistable mechanisms. A variety of thin film materials can be exploited and adequate geometry designs provide access to a vast design space [4-6]. Buckling of suspended clamped-clamped beams is well-described through Euler's theory [7], and has been investigated in several experiments at the microscale [6,8].

Owing to its semiconductor and excellent mechanical properties, silicon has been the material of choice for integrated electronics and MEMS for several decades, and has more recently proven to be a suitable material for development of large-scale integration of photonics, currently driven by the demand in data centers [9]. In particular, implementation of large-scale integrated silicon photonic switches into data distribution nodes is expected to boost efficiency and reliability of data networks. Reliable large-scale on-chip switching networks are thus subject of current research and development efforts. Fast electro-optical modulators or mature thermo-optical switches offer compactness and compatibility with standard silicon photonics processes [10], however, scaling these technologies to high numbers of in- and output ports as required in current and future datacenter applications, will result in power hungry networks with challenges in temperature management, integration, and sophistication in the required electronics [11]. Thus, implementing a non-volatile switching unit with zero power consumption in the idle state allows for a new generation of low power reconfigurable silicon photonics switch networks.

Recent reports on non-volatile photonic integrated circuits have demonstrated implementation of Phase Change Materials (PCM) [12,13], focused on applications including phase control and optical delay networks, however, the compatibility with standard silicon photonics platforms has been limited so far. In contrast, the recent demonstrations of MEMS integration in photonics provide a suitable path for large-scale photonic switches and to more general large-scale reconfigurable photonic circuits. MEMS-based integrated silicon photonic components including switches [14], phase shifters [15], and grating couplers [16] have been demonstrated so far. Introducing mechanical bistability in silicon photonic MEMS technology enables zero-power consumption devices. In this work, we propose a design for a bistable silicon photonic MEMS switch array, making use of the residual compressive stress in polysilicon device layer and the otherwise identical microfabrication process flow of the previously demonstrated silicon photonics MEMS switch array [14].

2. BISTABLE SWITCH DESIGN

The previously demonstrated silicon photonic MEMS switch array [14] uses suspended adiabatic coupler waveguides fabricated in a deposited thin polysilicon layer. As-deposited polysilicon films typically present residual compressive stress [17]. By controlling the compressive stress in the deposited polysilicon layer, buckled structures can be realized by selectively etching a sacrificial layer and thus releasing the clamped-clamped beams [7]. By applying an electrostatic force the beam can be switched from one stable state to the other. We apply this idea to our previously introduced vertically moving coupled waveguide system on silicon photonics platform [14]. A schematic representation of an $N \times N$ square switch network is presented in Fig. 1(a), which encompasses N^2 nodes and switching units. Each switching unit as shown in Fig. 1(b) comprises a moving body with two adiabatic couplers, a 90$°$ waveguide bend, a set of vertical electrostatic comb drives, and the suspension beams. The straight part of the movable waveguides are tapered from 150 nm to 1 μm in width along 30 μm ensuring adiabatic full light transfer between the moving waveguide and the bus waveguide in ON state. A 90$°$ bent waveguide with width of 1 μm and radius of 15 μm connects the orthogonally arranged tapered waveguides.

The cross-section of the platform is shown in Fig. 1(c). The implemented silicon photonics MEMS technology exhibits two possible thicknesses in the polysilicon layer, 100 nm and 300 nm, which can both be used for freestanding and movable components. The polysilicon movable waveguides are of ridge type with a ridge height of 200 nm and a total height of 300 nm. For the electrostatic actuation, 300 nm thick comb drive fingers with width of 1 μm, length of 4 μm, and pitch of 3 μm are included on each side of the straight part of the movable waveguides. As optical simulations have shown and as confirmed by previous experimental results, a vertical gap of g=300 nm between the bus waveguide and the movable waveguide is sufficient to prevent coupling; this distance will thus define the minimum required buckling amplitude d_0 for the optical switching as illustrated in Fig. 1(c). Here, we focus on the mechanical design of the bistable switch and for details of the optical design we refer to [14,18]. The amount of residual compressive stress and the geometry of the suspension beams will define deflection amplitude of the beams upon release. In our design, the moving waveguides are connected to a set of four pre-stressed suspension beams with length of 30 μm, height of 100 nm, and width of 1 μm each. As shown in Fig. 1(c) the platform from bottom to top includes: a silicon handle layer, 3 μm thick buried oxide (BOX), 220 nm crystalline device layer for passive components, a sacrificial oxide layer, and a 300 nm thick polysilicon layer for the movable waveguides, the suspensions and the actuators, respectively. After the final release process, the pre-stressed suspension beams will buckle into either one of the buckling states (switch ON or OFF). To trigger switching, a bias voltage is applied to the vertical electrostatic comb drive actuators which will allow to move the movable waveguides to either the ON or the OFF state. For an optimized low-loss waveguide coupling in the ON state, the vertical gap between the waveguides is set to 185 nm which is precisely controlled by mechanical stoppers.
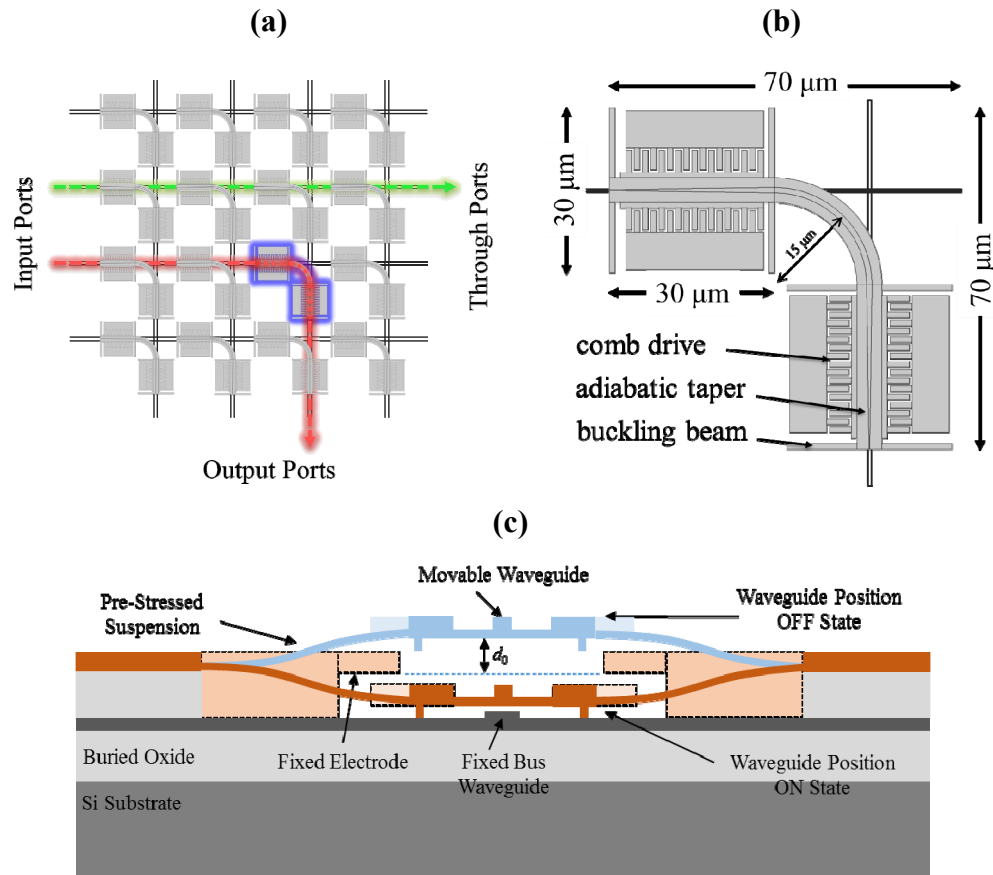
Figure 1. a) Bistable switch network. b) Bistable switch unit. c) Cross-section of the bistable switch in ON and OFF states.

3. SIMULATION RESULTS

3.1 Mechanical simulation

In a first step, we predict the buckling amplitude of the suspended pre-stressed beams for amounts of compressive stress that are typically accessible in CVD-deposited polysilicon thin films. The buckling amplitude will determine at the same time the initial gap between the waveguides in OFF state, as well as the amount of the required electromechanical force (and thus the actuation voltage) to actuate the switch. In order to prevent coupling between the fixed bus waveguide and the movable adiabatic coupler waveguide, the gap between the waveguides needs to exceed 300 nm. Therefore, the thickness of the sacrificial oxide plus the buckling amplitude should exceed 300 nm. An additional requirement for efficient coupling in the ON-state is a uniform gap or positioning of the movable waveguide in the coupling region. In order to predict the effect of the bi-axial thin film stress on the complex geometry including the straight waveguides and 90° bend, comb drives, as well as the suspensions, we have modeled the suspended structure in Comsol Multiphysics, and used the finite element method (FEM) solver to predict the buckling profile of the suspended structure for a compressive stress ranging from 0 MPa to 300 MPa. Fig. 2(a) represents the deformation of the released structure for a compressive stress ranging from 0 MPa to 60 MPa. The plot shows the vertical displacement of two probe points (point 1 and point 2) on the structure, revealing uniform deflection of the structure in the waveguide plane. The FEM simulation predicts a critical stress of 6 MPa, at which buckling begins, which is in accordance with the theoretical model for an individual clamped-clamped beam with the same dimensions (5.85 MPa). With increasing stress, the deformation due to buckling increases rapidly and exceeds 50 nm already at 10 MPa, as shown in Fig. 2(a). The

simulations predict, that a compressive stress of 60 MPa results in a buckling amplitude of d_0=280 nm. This buckling amplitude results in a total 745 nm ($2d_0$+185 nm) of vertical gap in the OFF state of the switch.

In a second step, we use the resulting deformed shape of the buckled structure to perform post-buckling simulations to estimate the required threshold force for switching and the corresponding critical vertical displacement. Fig. 2(b) shows the displacement of three probe points on the moving structure under application of a mechanical force on the comb drive fingers. The structure is initially stable in d_0=280 nm; by slowly increasing the distributed mechanical load on the comb drive fingers, the structure begins to move in vertical direction towards the fixed waveguide. After a displacement of 100 nm under an applied force of 0.15 µN, the waveguide suddenly jumps to the lower branch of the stability curve. By increasing the applied force, the beam's strain energy density increases and eventually approaches a maximum at the critical deflection amplitude of d_{cr}=100 nm. In this unstable state the strain energy is released suddenly and the beam bounces to the second (stable) bifurcation branch, with a deflection amplitude of $-d_0$ (= - 280 nm). The two stable states and an intermediate unstable state are shown in Fig. 2(c). Note that in the stable states, the buckled suspension beams exhibit a Cosine profile, while they follow a Sine profile in the transition, which corresponds to predictions by theory for clamped-clamped beams [7].
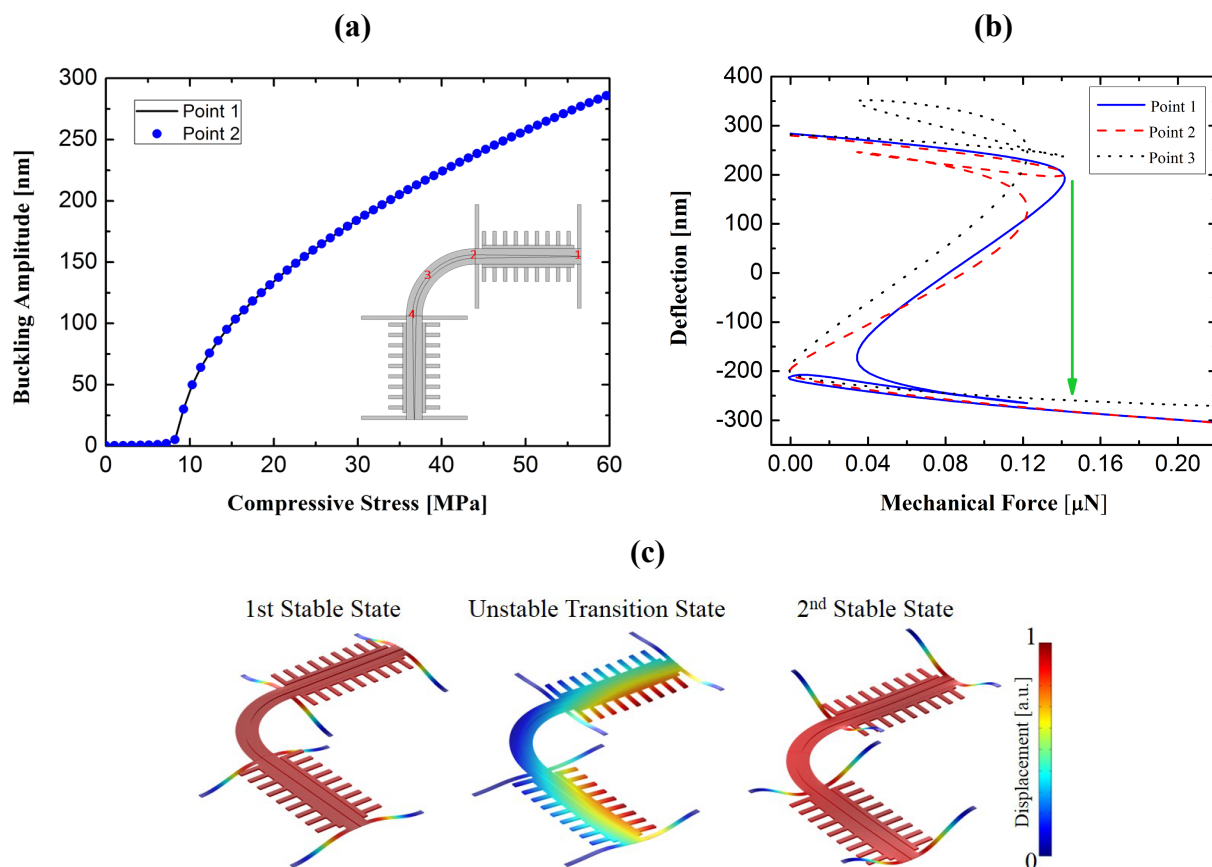
(a)　　　　　　　　　　　　　　　　　　　　　**(b)**

(c)

Figure 2. a) After-release buckling amplitude versus the residual compressive stress tracked for two selected points on the movable waveguide structure. Four displacement probe points are labeled in the inset. b) Out of plane deflection amplitude versus the applied mechanical force. c) Exaggerated displacement profile of the switch in its two stable states and an unstable state.

3.2 Electromechanical simulation

Finally, we set up a coupled electromechanical multiphysics FEM simulation to investigate the displacement of the movable structure when applying an actuation voltage to the fixed combs of the electrostatic comb drive actuators. The applied voltage profile is shown in Fig. 3(a). We extract the deformation profile of the structure under various applied voltages and probe the vertical displacement at selected probe points of the movable waveguide structure. Fig. 3(b) presents the electromechanical simulation results for a structure with initial stable buckling amplitude of 280 nm. When increasing the applied voltage, the movable waveguides are displaced towards the fixed waveguide. The amount of displacement depends on the position on the movable structure as indicated by the selected probe points in Fig. 3(b). After a continuous increase in the displacement, the critical deflection is reached, and the buckled beam switches suddenly from one stable position to the other. For our design with initial compressive stress of 60 MPa this instability happens for an actuation voltage of 28 V, which corresponds to a total electrostatic force of ~ 0.26 μN exerted on the comb drive.

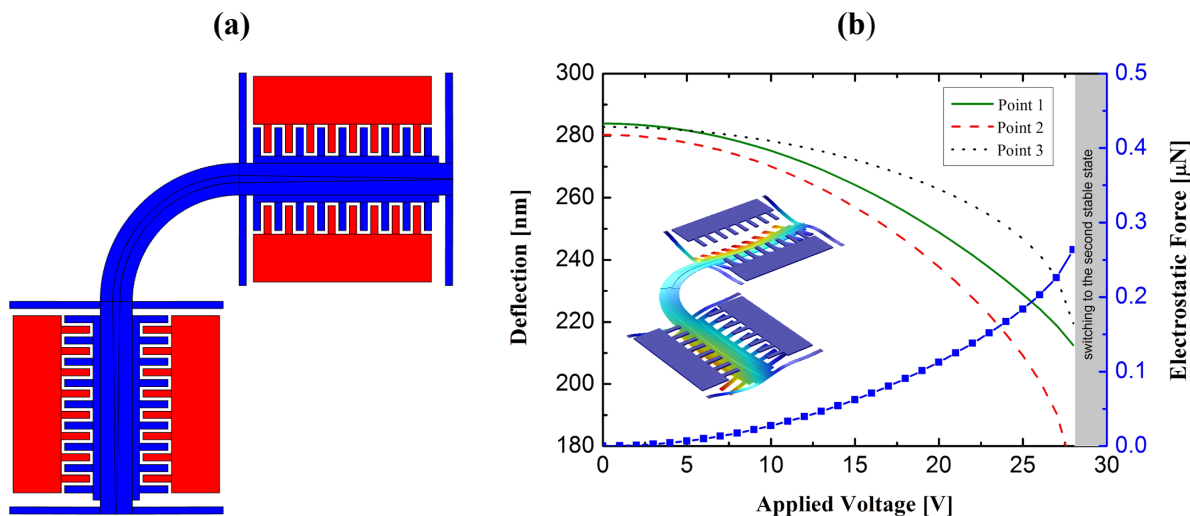**(a)**   **(b)**

Figure 3. a) Applied voltage profile on the actuator (red and blue define maximum and minimum, respectively). b) Point probe deflection for three points on the moving structure and the total exerted electrostatic force versus the applied voltage on the actuator. The deformation of the structure in the instable transient phase is shown in the inset.

4. BUCKLING DEMONSTRATION

In order to confirm our FEM simulation results and to validate the concept of bistability in the proposed complex geometry, we have fabricated a representative experimental demonstrator. Prior to fabrication of the structure, we deposited 100 nm of poly-silicon on an oxidized silicon test wafer and measured the compressive stress of the deposited layer by comparing the wafer bow before and after the deposition. For our deposited layer (100 nm, at ~610 °C, in LPCVD centrotherm poly tube) we measure a compressive stress of 275 MPa ± 25 MPa. Based on our FEM simulations, the proposed design will buckle with amplitude of ~ 650 nm for compressive stress of ~275 MPa, which is more than sufficient for the switching action that requires enough vertical distance between the bus and coupling waveguide in OFF state. In this preliminary experiment, we did not focus on the precise control of the compressive stress, however, suitable techniques for stress control by annealing are well understood [17] and can readily be implemented in the fabrication process.

The fabrication process steps are shown in Fig. 4. Starting with a 1 μm thick oxidized silicon wafer, anchors were first patterned with a full etch of the oxide layer. Next, a 100 nm thick layer of polysilicon was deposited, and etched to form the movable structures. Finally, the suspended structures were released by an HF vapor etch step. All photolithography steps were performed using direct laser writing (Heildelberg Instruments VPG200) and are not presented in Fig. 4. We have evaluated the residual stress in the released structures using geometrical parametric sweep of the structures, and comparing to the theoretical and simulation results.
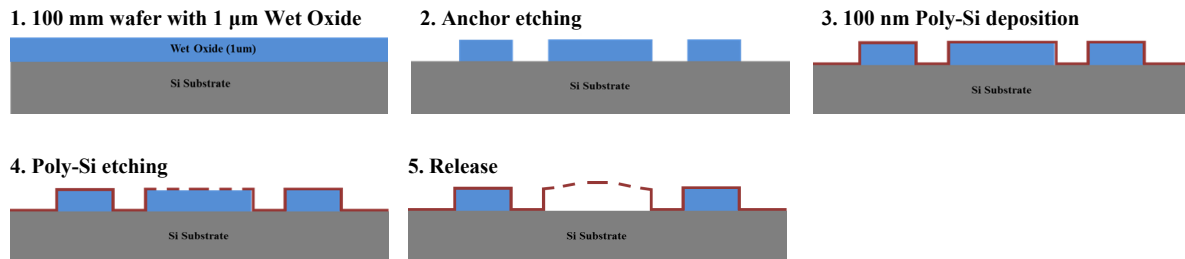
Figure 4. Fabrication process steps for realizing buckling mechanism demonstrators.

The SEM micrographs of the buckled demonstrator structures are shown in Fig. 5. The fabrication yielded both up-buckled and down-buckled structures, as shown in Fig. 5(a) and Fig. 5(b) respectively. Up- or down-buckling occurs spontaneously and depends on local variations of the initial conditions in stress and geometry. A close-up view of the buckled structures reveals details of the profile validating the results of the FEM buckling mode study; uniform elevation of the up-buckled structures and a well-defined etch undercut of ~2.5 μm is apparent from the SEM images. The down-buckled structures are further positioned uniformly over the substrate. The tilted view close up reveals a narrow gap between the moving body and the substrate.
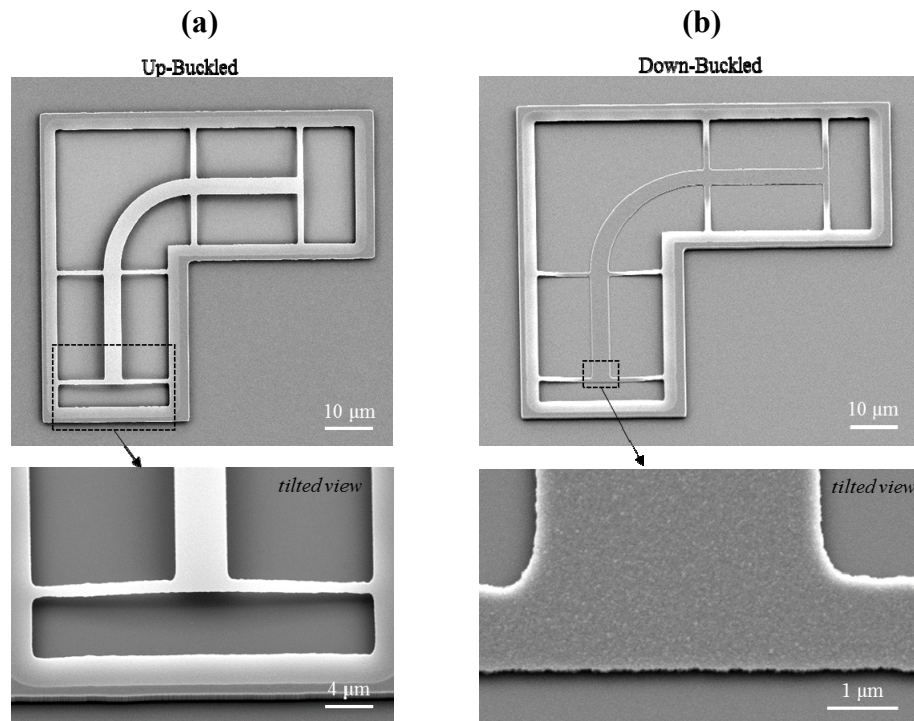

Figure 5. SEM micrographs of: a) an up-buckled structure with a zoomed tilted view of one of the suspension areas showing the buckled beam profile and the undercut region. b) A down-buckled structure with a zoomed tilted view of one of two ends of the structure revealing a narrow gap between the vertically moving body and the substrate.

Finally, we used optical profilometry based on vertical scanning interferometry (Veeco Wyko NT1100) to measure the buckling amplitude of the test structures. The inspection results for a down-buckled structure are shown in Fig. 6(a). The cross-section profiles for two selected profile lines in Fig. 6(a) are plotted in Fig. 6 (b). The measurements reveal an average buckling amplitude of 800 nm; the indicated step of 200 nm height in the cross-section profile accounts for 100 nm of the poly-silicon thickness plus 100 nm of the air gap between the buckled structure and the substrate.

Considering a poly-silicon layer deposition on a 1 μm thick sacrificial oxide, we conclude on 800 nm buckling amplitude. This exceeds our FEM predictions (650 nm) by 150 nm, which we attribute to non-ideal boundary conditions due to the undercut of the anchors of the released structures.

(a)   **(b)**
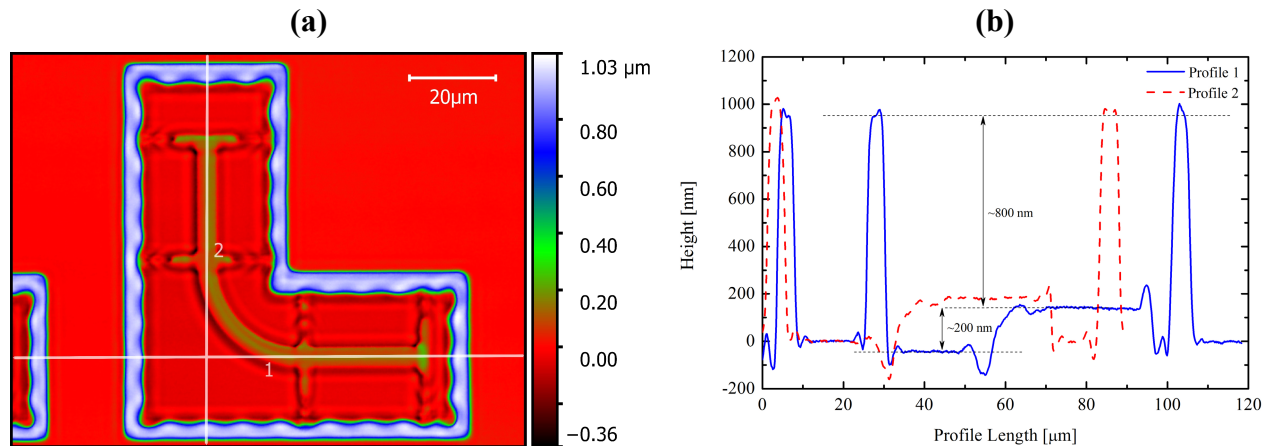

Figure 6. a) The color map profile of the down-buckled structure obtained from the vertical scanning interferometry. b) Cross-section graphs along the profile lines defined in Fig. 6(a). The graphs give ~800 nm of buckling amplitude.

5.   CONCLUSION

We have proposed a design for a bistable silicon photonic MEMS switch, exploiting compressive residual stress in suspended polysilicon beams to address both non-volatile ON and OFF states. We have demonstrated the concept of bistability experimentally by fabricating a demonstrator of the proposed complex geometry. Our proposed switch design further includes a movable structure with adiabatically tapered waveguides, which is actuated by a set of vertical electrostatic comb drive actuators. Based on our FEM simulations, the movable structure can buckle out of plane to either stable state with ±280 nm of amplitude upon release of 60 MPa compressive stress in a clamped-clamped beam suspension design. FEM simulations of an integrated electrostatic vertical comb drive actuator design predict actuation at 28 V to switch between the stable ON and OFF states. We experimentally demonstrate the buckling of the geometry in both ON and OFF positions by selectively etching a sacrificial layer and thus releasing a polysilicon structure with compressive stress of 275 MPa. The buckling amplitude of our demonstrator is ~800 nm which in good agreement with both Euler's theory for clamped-clamped beams and with our FEM simulation. The implementation of the proposed mechanical bistability design in silicon photonic MEMS paves the way for non-volatile large-scale photonic switch matrices.

ACKNOWLEDGEMENTS

REFERENCES

[1] Charlot, B., Sun, W., Yamashita, K., Fujita, H., and Toshiyoshi, H., "Bistable nanowire for micromechanical memory," J Micromech Microeng, 18(4), 045005 (2008).

[2] Receveur, R. A., Marxer, C. R., Woering, R., Larik, V. C., and de Rooij, N. F., "Laterally moving bistable MEMS DC switch for biomedical applications," J Microelectromech Syst, 14(5), 1089-1098 (2005).

[3] Yang, Y. J., Liao, B. T., and Kuo, W. C., "A novel 2× 2 MEMS optical switch using the split cross-bar design," J Micromech Microeng, 17(5), 875-882 (2007).

[4] Guckel, H., Randazzo, T., and Burns, D. W., "A simple technique for the determination of mechanical strain in thin films with applications to polysilicon," J. Appl. Phys. 57(5), 1671-1675 (1985).

[5] Matoba, H., Toshio I., Kim, C-J., and Muller, R. S., "A bistable snapping microactuator," Proc. IEEE MEMS, 45-50 (1994).

[6] Saif, M. T. A., "On a tunable bistable MEMS-theory and experiment," J Microelectromech Syst, 9(2), 157-170 (2000).

[7] Fang, W., and Wickert, J. A., "Post buckling of micromachined beams," J Microelectromech Syst, 4(3), 116 (1994).

[8] Qiu, J., Lang, J. H., and Slocum, A. H., "A curved-beam bistable mechanism," J Microelectromech Syst, 13(2), 137-146 (2004).

[9] Rickman, A., "The commercialization of silicon photonics," Nat. Photon. 8(8), 579-582 (2014).

[10] Lee, B. G., Biberman, A., Chan, J., and Bergman, K., "High-performance modulators and switches for silicon photonic networks-on-chip," IEEE J. Sel. Top. Quantum Electron, 16(1), 6-22 (2010).

[11] Cheng, Q., Rumley, S., Bahadori, M., and Bergman, K., "Photonic switching in high performance datacenters," Opt. Express, 26(12), 16022-16043 (2018).

[12] Lankhorst, M. H., Ketelaars, B. W., and Wolters, R. A., "Low-cost and nanoscale non-volatile memory concept for future silicon chips," Nat. Mater., 4(4), 347 (2005).

[13] Ríos, C., Stegmaier, M., Hosseini, P., Wang, D., Scherer, T., Wright, C. D., Bhaskaran, H., and Pernice, W. H., "Integrated all-photonic non-volatile multi-level memory," Nat. Photonics, 9(11), 725 (2015).

[14] Seok, T. J., Quack, N., Han, S., Muller, R. S., and Wu, M. C., "Large-scale broadband digital silicon photonic switches with vertical adiabatic couplers," Optica, 3(1), 64-70 (2016).

[15] Fuchs, D. T., Chan, H. B., Stuart, H. R., Baumann, F., Greywall, D., Simon, M. E., and Wong-Foy, A., "Monolithic integration of MEMS-based phase shifters and optical waveguides in silicon-on-insulator," Electron. Lett., 40(2), 142-143 (2004).

[16] Errando-Herranz, C., Colangelo, M., Ahmed, S., Björk, J., and Gylfason, K. B., "MEMS tunable silicon photonic grating coupler for post-assembly optimization of fiber-to-chip coupling," Proc. IEEE MEMS, 293-296 (2017).

[17] Zhang, X., Zhang, T-Y., Wong, M., and Zohar, Y., "Residual-stress relaxation in polysilicon thin films by high-temperature rapid thermal annealing," Sens. Actuator A-Phys., 64(1), 109-115 (1998).

[18] Sattari, H., Graziosi, T., Kiss, M., Seok, T. J., Han, S., Wu, M. C., and Quack, N., "Analog silicon photonic MEMS phase-shifter with double-step electrostatic actuation," Proc. IEEE OMN, 1-2 (2017).